







DOI: <http://dx.doi.org/10.1590/1807-1929/agriambi.v26n6p466-476>

Predicting soybean grain yield using aerial drone images¹

Predição da produtividade de grãos de soja utilizando imagens aéreas de drone

Aderson S. de Andrade Júnior^{2*}, Silvestre P. da Silva³, Ingrid S. Setúbal³,
Henrique A. de Souza², Paulo F. de M. J. Vieira² & Raphael A. das C. N. Casari⁴

¹ Research developed at Embrapa Meio-Norte, Teresina, PI, Brazil

² Embrapa Meio-Norte, Teresina, PI, Brazil

³ Universidade Federal do Piauí/Programa de Pós-Graduação em Agronomia, Teresina, PI, Brazil

⁴ Embrapa Agroenergia, Brasília, DF, Brazil

HIGHLIGHTS:

Prediction models based on VIs using the red, NIR and red edge bands better explained the variability in soybean grain yield.

The variability of soybean grain yield was due more to water regimes than nitrogen supplementation.

The soybean grain yield prediction model generated with the EVI-2 VI showed greater accuracy and spatial randomness.

ABSTRACT: This study aimed to evaluate the ability of vegetation indices (VIs) obtained from unmanned aerial vehicle (UAV) images to estimate soybean grain yield under soil and climate conditions in the Teresina microregion, Piauí state (PI), Brazil. Soybean cv. BRS-8980 was evaluated in stage R5 and submitted to two water regimes (WR) (100 and 50% of crop evapotranspiration - ETc) and two N levels (with and without N supplementation). A randomized block design in a split-plot scheme was used, in which the plots were the water regimes and the subplots N levels, with five replicates. Each plot contained twenty 4.5 m-long rows, spaced 0.5 m apart, with a total area of 45 and 6 m² study area for grain yield evaluations. Twenty VIs obtained from multispectral aerial images were evaluated and correlated with grain yield measurements in the field. Pearson's correlation, linear regression, and spatial autocorrelation (Global and Local Moran's I) were used to analyze the performance of the VIs in predicting grain yield. The R², RMSE and nRMSE indices were used to validate the linear regression models. The prediction model based on EVI-2 exhibited high spatial randomness for all the treatments, and smaller prediction errors of 149.68 and 173.96 kg ha⁻¹ (without and with N supplementation, respectively).

Key words: *Glycine max* L., remotely piloted aircraft, vegetation indices, autocorrelation, Moran's I

RESUMO: O estudo objetivou avaliar a capacidade de índices de vegetação (IV) obtidos de imagens aéreas por veículo aéreo não tripulado em estimar a produtividade de grãos de soja, nas condições de solo e clima da microrregião de Teresina, Piauí, Brasil. Avaliou-se a cultivar de soja BRS-8980, em estágio R5, submetida a dois regimes hídricos (RH) (100 e 50% da evapotranspiração da cultura - ETc) e dois níveis de N (com e sem suplementação de N). O delineamento experimental foi o de blocos ao acaso, em parcelas subdivididas, sendo as parcelas os regimes hídricos e as subparcelas os níveis de nitrogênio, com cinco repetições. Cada parcela continha 20 linhas de 4,5 m de comprimento, espaçadas de 0,5 m entre linhas, com área de 45 m² e uma área útil para avaliação da produtividade de grãos de 6 m². Avaliaram-se 20 IV obtidos de imagens aéreas de câmera multiespectral, os quais foram correlacionados com medidas de produtividade de grãos em campo. Adotaram-se análises de correlação de Pearson, de regressão linear e de autocorrelação espacial (índice I de Moran global e local) para geração e análise de desempenho dos IV na predição da produtividade de grãos. Para validação dos modelos de regressão linear, usou-se os índices R², RMSE e nRMSE. O modelo de predição baseado no EVI-2 apresenta elevada aleatoriedade espacial, para todos os tratamentos avaliados, e menores erros de predição iguais a 149,68 kg ha⁻¹ (sem suplementação de N) e 173,96 kg ha⁻¹ (com suplementação de N).

Palavras-chave: *Glycine max* L., aeronave remotamente pilotada, índices de vegetação, autocorrelação, Moran's I

• Ref. 256489 – Received 20 Sept, 2021

* Corresponding author - E-mail: aderson.andrade@embrapa.br

• Accepted 12 Jan, 2022 • Published 04 Feb, 2022

Editors: Lauriane Almeida dos Anjos Soares & Hans Raj Gheyi

This is an open-access article distributed under the Creative Commons Attribution 4.0 International License.



INTRODUCTION

It is important to develop crop yield prediction models because they enable crop conditions to be monitored in the field and previous adoption of management practices aimed at achieving high yields (Silva Junior et al., 2018).

Remote sensing is a promising technique that allows the accurate, low-cost prediction of the biophysical and biochemical parameters of plants. The high yield and spatial accuracy in predicting these characteristics using unmanned aerial vehicles (UAV) images can help assess genotype behavior and management practices, detect biotic and abiotic stress, and predict crop yield, contributing to decision-making by producers (Barbedo, 2019).

The use of vegetation indices (VIs) is common in remote sensing studies. VIs are reliable algorithms for evaluating plant cover, vigor and growth dynamics, and nutritional status, among other applications (Xue & Su, 2017), making them a promising tool for crop yield prediction (Zhao et al., 2020).

Several studies have reported a correlation between VIs and yield in crops such as corn, wheat, cotton, and rice (Dong et al., 2015; Baio et al., 2018; Hassan et al., 2019; Zhao et al., 2020). Holzman et al. (2014), Christenson et al. (2016), Silva Junior et al. (2018), Maimaitijiang et al. (2020), and Schwalbert et al. (2020) conducted studies with soybean and concluded that VIs produced satisfactory and promising results for predicting soybean yield. However, studies in this area are still incipient in the Mid-North region of Brazil.

The present study aimed to evaluate the ability of vegetation indices (VIs) obtained from unmanned aerial vehicle (UAV) images to estimate soybean grain yield under the soil and climate conditions of the Teresina microregion, Piauí state (PI), Brazil.

MATERIAL AND METHODS

The experiment was conducted at Embrapa Mid-North in Teresina, Piauí state, Brazil (05° 02' 13" S, 42° 47' 49" W, and altitude of 72 m), from July to November 2019 (Figure 1). The climate in the region is classified as Aw, with a wet summer and dry winter (Medeiros et al., 2020). Average annual temperature and rainfall are 27.4 °C and 1,325 mm, respectively, with the latter concentrated between January and May (INMET, 2020). During the experimental period, the average maximum and minimum temperatures, and cumulative rainfall were 29.6°C, 27.8 °C and 18.6 mm, respectively. At the time of the flight (11:00 a.m.-12:00 p.m.), average maximum and minimum temperature, wind speed, and global solar radiation were

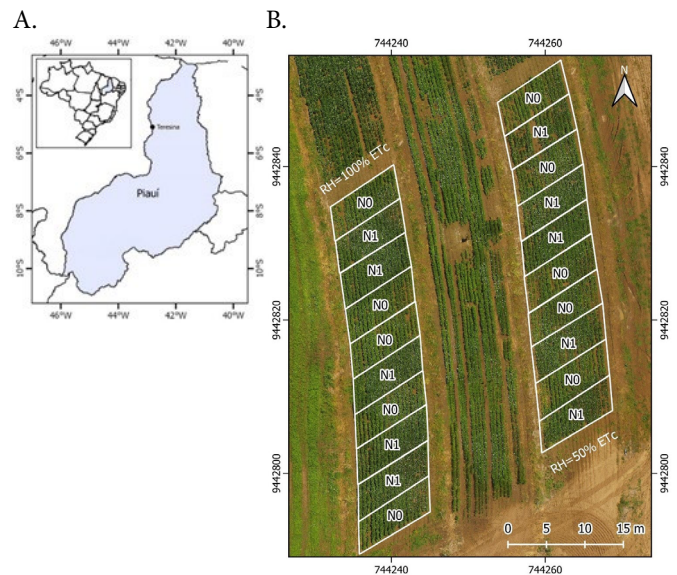


Figure 1. Location (A) and details of the experimental area (B)

30.7°C, 29.3 °C, 2.8 m s⁻¹, and 406.8 W m⁻², respectively (INMET, 2020).

The soil at the experimental site is classified as eutrophic Ultisol (Melo et al., 2014) (Table 1). Fertilization management was based on the soil chemical properties. Nitrogen (urea), phosphorus (simple superphosphate), and potassium (potassium chloride) were applied to the soil and micronutrients to the leaves (Silva, 2021). A 1,000 kg N ha⁻¹ dose was applied to meet soybean N requirements throughout the crop season in order to achieve maximum productive potential, with an expected grain yield of 6 Mg ha⁻¹. For each Mg of soybean produced, 80 kg ha⁻¹ of nitrogen is needed and nitrogen fertilization efficiency is estimated at 50% (Hungria et al., 2001).

The BRS-8980 soybean cultivar (Embrapa) with a determinate growth habit, GM 8.9, and a 125-136-day growing season was used. A randomized block design in a split-plot scheme was adopted, in which the plots were the following water regimes: deficit WR (50% replacement of crop evapotranspiration-ETc) (I0) and full WR (100% replacement of ETc) (I1), and the subplots were the levels of nitrogen fertilization: without nitrogen (N0) and with nitrogen (1000 kg ha⁻¹) (N1), resulting in four treatments (I0N0, I0N1, I1N0, and I1N1), with five replicates. Each plot contained twenty 4-5 m-long rows, spaced 0.5 m apart, with a total area of 45 m² and 6 m² study area for grain yield evaluations.

Sowing was performed manually on 23/07/2019, distributing 20 seeds per meter in the furrow. The seeds were inoculated with *Bradyrhizobium japonicum* (SEMIA 5079 and 5080), at a ratio of 100 mL of inoculant to 7 kg of seeds. After

Table 1. Soil chemical and granulometric properties in the experimental area

Layer (m)	Sand		Fine Sand		Silt	Clay		Textural classification		
	(g kg ⁻¹)									
0-0.20	267.3	470.6	116.0	146.1	Sandy loam					
0.20-0.40	231.6	424.0	105.5	238.9	Sandy clay loam					
	P	K	Ca	Mg	H + Al	SB	CEC	OM	S	pH
	(mg dm ⁻³)				(cmol _c dm ⁻³)			(dag kg ⁻¹)	(%)	(CaCl ₂)
0-0.20	10.15	0.23	2.40	0.83	1.18	3.45	4.63	1.03	74.5	5.50
0.20-0.40	5.41	0.22	2.63	0.83	1.34	3.68	5.01	0.91	73.4	5.38

P - Phosphorus; K - Potassium; Ca - Calcium; Mg - Magnesium; H + Al - Potential acidity; SB - Sum of bases; CEC - Cation exchange capacity; OM - Organic matter; S% - Base saturation; pH (CaCl₂) - pH in calcium chloride

germination, the seedlings were thinned, leaving 10 to 12 plants per linear m^{-1} . Harvesting was performed at 113 days after sowing (DAS) (13/11/2019) at the beginning of the R8 phase, cutting the plants in the four 3 m-long center rows spaced 0.5 m apart ($6 m^2$ per plot).

Irrigation management was performed based on crop evapotranspiration (ET_c) replacement. The reference evapotranspiration (ET_o) was estimated by the Penman-Monteith method (Allen et al., 1998) using global solar radiation data ($MJ m^{-2}$), air temperature ($^{\circ}C$), relative air humidity (%), and wind speed ($m s^{-1}$) obtained from an automatic agro-meteorological station located 500 m from the experimental area. The soybean crop coefficients proposed by the FAO (Allen et al., 1998) were used to estimate ET_c. Irrigation was applied using a conventional fixed sprinkler system, with sprinklers spaced 12 m apart. Irrigation depth was controlled by installing two blocks of 12 collectors each, one in each water regime, spaced 3 m between the lateral lines of sprinklers, in the center of the experimental plot.

From sowing to stage V3, full irrigation was used for both treatments, followed by the application of different water regimes from stages V4 to R5, with 50 and 100% ET_c replacement. After stage R5, full irrigation was resumed for all treatments. The cumulative irrigation depth during the soybean season in each water regime are shown in Table 2.

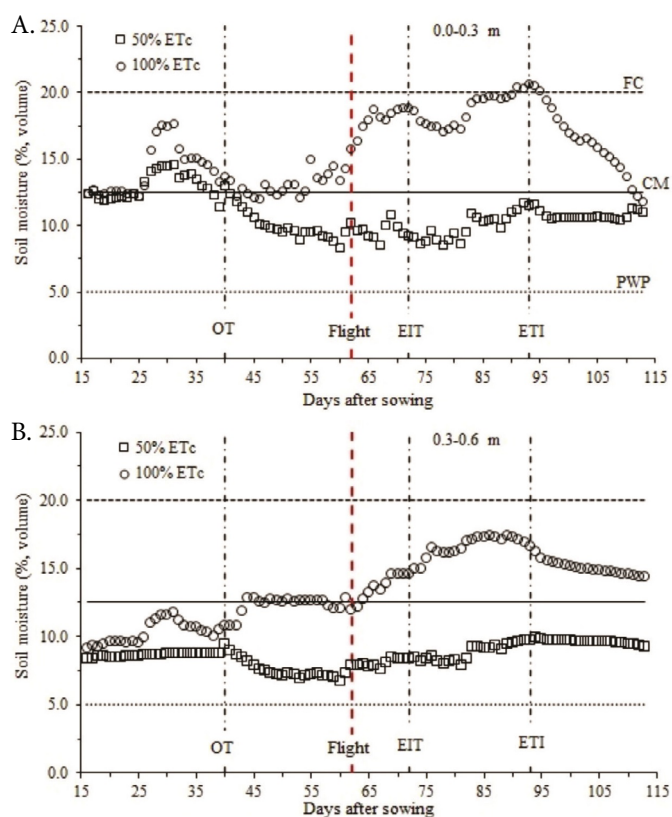
Soil moisture content was monitored using Campbell CS616 probes, with three probes in each water regime, two 0-0.30 m and one 0.30-0.60 m deep, with continuous moisture data acquisition and recording by a CR1000 datalogger. From the onset of irrigation until the application of differentiated water regimes (OT), average moisture content in the 0-0.30 m layer ranged between 13.0 and 14.2% in the treatments with 50 and 100% ET_c, while in the 0.30-0.60 layer, variation was 8.6% (50% ET_c) and 10.3% (100% ET_c) (Figure 2).

Average moisture content in the 0-0.30 m layer under the different water regimes (OT-ET) was 9.9 and 14.7% in the treatments with 50 and 100% ET_c respectively, and 7.7% (50% ET_c) and 12.7% (100% ET_c) in the 0.30-0.60 m layer. From the beginning of irrigation until the flight date (62 DAS), average moisture content in the 0-0.30 m layer was 10.0 and 13.2% in the treatments with 50 and 100% ET_c, respectively, and 7.6% (50% ET_c) and 12.3% (100% ET_c) in the 0.30-0.60 m layer (Figure 2). These data indicate that in the full irrigation WR, soil moisture was maintained at higher-than-critical levels to allow adequate soybean development and production. Under deficit irrigation WR, values below the critical moisture content and above the permanent wilting point were recorded during the study period, which is a limiting factor for soybean grain development and yield.

Table 2. Cumulative irrigation depth (mm) in each water regime during the soybean crop season

WR (% ET _c)	S-OT	OT-FD	OT-ET	ET-EIT	Season
50	125.3	84.0	90.6	56.1	356.0
100	127.1	159.4	167.7	57.7	511.9

WR - Water regimes (% ET_c); S - Sowing date; OT - Onset of differentiated WR treatment (40 DAS); FD - Flight date (62 DAS); ET - End of differentiated WR treatment (72 DAS); EIT - End of irrigation treatment (93 DAS)



FC - Field capacity; CM - Critical moisture; PWP - Permanent wilting point; OT - Onset of differentiated WR treatment (40 DAS); ET - End of differentiated WR treatment (72 DAS); EIT - End of irrigation treatment (93 DAS); Flight - Flight date (62 DAS)

Figure 2. Soil moisture content during the soybean season in the 0-0.30 and 0.30-0.60 m layers in response to the water regimes applied

An XFLY X800 hexacopter (Xfly Brasil, Bauru, SP) UAV was used to obtain aerial images. A flight was performed on 24/09/2019, at 62 DAS, between 11:00 a.m. and 12:00 p.m. The flight was planned using Pix4D Capture[®] software (www.pix4d.com). The flight plan was created to ensure that the images were captured with an 80% lateral and frontal overlap, maintaining the flight line at 30 m above ground level, with GSD (ground sample distance) of ≈ 1.5 cm pixel⁻¹.

The multispectral images were acquired by a RedEdge Micasense sensor, capable of capturing five spectral bands: Red (668 nm), Green (560 nm), Blue (475 nm), NIR (840 nm), and RedEdge (717 nm). The images generated were georeferenced and corrected using GPS and the solar radiation sensor installed on the top of the aircraft. A radiometric calibration standard was also used to correct the images, which were saved in 16-bit tiff format. The orthomosaic images were produced with Pix4D Mapper[®] software.

The orthomosaic underwent a supervised classification process (maximum likelihood method), allowing the rasterization of the orthomosaic into two classes (soil and leaves). This enabled the removal of pixels classified as mosaic soil, ensuring that the VIs were estimated only with pixels classified as leaves. The process was performed using the Semi-Automatic Classification (SCP) plug-in of QGIS v. 3.16 (QGIS, 2021). The vector layer containing the pixels classified as leaves was subdivided into two equal parts, thus obtaining two distinct datasets for the training and validation phases of the VIs. The "Split Polygon" plug-in of QGIS v. 3.16 (QGIS, 2021) was used.

The spectral response of the soybean to the treatments was quantified using 20 VIs estimated from the multispectral image bands (R, G, B, red edge, and NIR) (Table 3). The multispectral indices were estimated with QGIS v. 3.16 (QGIS, 2021). The VI values of each subplot were extracted with the zonal statistics plugin of QGIS v. 3.16 (QGIS, 2021). To that end, the vector layer of the subplots was used, containing only the areas classified as leaves, subdivided into two equal parts (modeling and validation).

The strategy adopted for statistical analysis of the data consisted of the following steps: a) Pearson's correlation analysis between grain yield data, measured in the plots, and the 20 VIs evaluated, also extracted at the experimental plot level, aimed at pre-selecting the most promising indices ($r \geq 0.8$); b) creation of grain yield prediction models using the most promising VIs via linear regression analysis, applying the coefficient of determination (R^2) (Eq. 1) and standard error of estimate (SEE) as the selection criteria (Eq. 2); c) validation of grain yield prediction models applying R^2 , root mean square error (RMSE) (Eq. 3) and normalized root mean square error (nRMSE) (Eq. 4), using a different dataset different from that employed in creating the models and d) spatial autocorrelation analysis of

the most promising prediction models, from steps a, b and c, through Moran's global index (Eq. 5) and Moran's local index (Eq. 6) (Anselin, 1995), using the residuals of grain yield prediction models (RMR) (Eq. 7) to assess the degree of model randomness, as recommended by Maimaitijiang et al. (2020). For the estimates of R^2 , SEE, RMSE, and nRMSE, the Excel Real Statistics Resource Pack (version 7.6) supplement was used (Zaiontz, 2020).

$$R^2 = \frac{\sum_{i=1}^n (\hat{Y}_i - \hat{Y}_m)^2}{\sum_{i=1}^n (Y_i - \bar{Y}_i)^2} \tag{1}$$

$$SEE = \sqrt{\frac{\sum_{i=1}^n (Y_i - \hat{Y}_i)^2}{n - 2}} \tag{2}$$

$$RMSE = \sqrt{\frac{\sum_{i=1}^n (Y_i - \hat{Y}_i)^2}{n - 1}} \tag{3}$$

Table 3. Multispectral vegetation indices evaluated in the study

Bands/Indices	Acronym	Equation	Reference
Chlorophyll index red	CI-RED	$\frac{R_n}{R_r} - 1$	Gitelson et al. (2005)
Chlorophyll vegetation index	CVI	$\frac{R_n R_r}{R_g^2}$	Vincini et al. (2008)
Enhanced vegetation index	EVI	$\frac{2,5(R_n - R_r)}{R_n + 6R_r - 7,5R_b + 1}$	Gitelson et al. (2005)
Two-band enhanced vegetation index	EVI-2	$\frac{2,5(R_n - R_r)}{R_n + 2,4R_r + 1}$	Jiang et al. (2008)
Green chlorophyll index	GCI	$\frac{R_n}{R_g} - 1$	Gitelson et al. (2005)
Green normalized difference vegetation	GNDVI	$\frac{R_n - R_g}{R_n + R_g}$	Hunt & Daughtry (2018)
Green ratio vegetation index	GRVI	$\frac{R_n}{R_g}$	Sripada et al. (2006)
Modified excess green	MEXG	$1,262R_g - 0,884R_r - 0,311R_b$	Burgos-Artizzu et al. (2011)
Modified normalized green red difference	MNGRD	$\frac{R_g^2 - R_r^2}{R_g^2 + R_r^2}$	Bendig et al. (2015)
Normalized difference Red-Edge	NDRE	$\frac{R_n - R_{RE}}{R_n + R_{RE}}$	Wang et al. (2014)
Normalized difference vegetation index	NDVI	$\frac{R_n - R_r}{R_n + R_r}$	Gitelson et al. (2005)
Normalized green red difference	NGRD	$\frac{R_g - R_r}{R_g + R_r}$	Hamuda et al. (2016)
Optimized Soil Adjusted Vegetation Index	OSAVI	$\frac{R_n - R_r}{R_n + R_r + 0,16}$	Roundeaux et al. (1996)
Pigment-specific normalized difference index	PSND	$\frac{R_n - R_b}{R_n + R_b}$	Blackburn (1998)
Renormalized Difference Vegetation Index	RDVI	$\frac{R_n - R_r}{(R_n - R_r)^{0,5}}$	Roujean & Breon (1995)
Red-Edge chlorophyll index	RECI	$\frac{R_n}{R_{RE}} - 1$	Gitelson et al. (2005)
Ratio vegetation index	RVI	$\frac{R_n}{R_r}$	Gitelson et al. (2005)
Soil Adjusted Vegetation Index	SAVI	$\frac{1,5(R_n - R_r)}{(R_n + R_r + 0,5)}$	Zhong et al. (2019)
Simplified canopy chlorophyll content index	SCCCI	$\frac{NDRE}{NDVI}$	Raper & Varco (2015)
Triangular greenness index	TGI	$R_g - (0,39R_r) - (0,61R_b)$	Hunt et al. (2011)

R_n - Spectral reflectance - near infrared (840 nm); R_g - Spectral reflectance - green (560 nm); R_{RE} - Spectral reflectance - near red (717 nm); R_r - Spectral reflectance red (668 nm) and R_b - Spectral reflectance - blue (475 nm)

$$nRMSE = \frac{RMSE}{(\bar{Y}_i)} 100 \tag{4}$$

$$I = \frac{n \sum_{i=1}^n \sum_{j=1}^n W_{ij} (y_i - \bar{y})(y_j - \bar{y})}{\sum_{i=1}^n \sum_{j=1}^n W_{ij} \sum_{i=1}^n (y_i - \bar{y})^2} \tag{5}$$

$$I_{(i)} = \frac{(y_i - \bar{y}) \sum_{j=1}^n (y_j - \bar{y})}{\sum_{i=1}^n (y_i - \bar{y})^2} \tag{6}$$

$$W_{ij} = RMR = Y_i - \hat{Y}_i \tag{7}$$

where:

- n - number of observations;
- Y_i - GY values measured in the field;
- \hat{Y}_i - GY values estimated by linear regression models;
- Y_m - mean of the GY values estimated by the linear regression models;
- \bar{Y}_i - mean of the GY values measured in the field;
- W_{ij} - spatial matrix of weighting between i and j;
- y_i - GY prediction error of the vegetation index in area i;
- y_j - GY prediction error of the vegetation index in area j; and,
- y - mean of the GY values estimated by the regression models.

The RMSE relates the magnitude of the observed values versus those estimated by the models, while the nRMSE is a normalized measure of the RMSE used to compare the performance of different regression models (Maimaitijiang et al., 2020). Moran's global index has been shown to be efficient in evaluating the spatial autocorrelation of regression models (Dalposso et al., 2013; Ghulam et al., 2015). Moran's I values range from -1 to 1, demonstrating negative to positive spatial autocorrelation, respectively, with zero indicating randomness, where greater randomness denotes better regression model performance (Maimaitijiang et al., 2020).

To estimate Moran's global I, the experimental plots were subdivided into seven polygons, with areas approximately equal to those used to quantify GY in the field. The "Split Polygon" plug-in of QGIS v. 3.16 (QGIS, 2021) was used. The global and local Moran's I were estimated using GeoDA software (Anselin et al., 2006). The nearest neighbor's method was applied to weight the autocorrelation spatial matrix. The statistical pseudo-p-values of Moran's local index were obtained using

999 random permutations. The number of 69 (for N treatments separately) and 139 (for all treatments) nearest neighbors was defined, making it possible for the RMR of each sub-plot to be compared with all the others.

RESULTS AND DISCUSSION

Pearson's correlation shows the interaction between soybean grain yield and VIs (Table 4). There was greater positive interaction between GY and the RECI, EVI, EVI-2, OSAVI, SAVI, and GCI VIs, and low interaction between the MEXG, MNGRD, and TGI and GY VIs (Table 4).

The correlation shows the similarity between the VIs that use the same spectral bands, such as EVI, EVI-2, NDRE, and RECI, which use the red, NIR, and red-edge bands in their estimations, as well as the SAVI and OSAVI, which correct the soil effect on the vegetation signal (Nguy-Robertson et al., 2012; Silva Junior et al., 2018). The highest Pearson correlation values ($r \geq 0.8$) were obtained for EVI, EVI-2, RDVI, SAVI, and OSAVI (Table 4).

Silva Junior et al. (2018) found a high correlation between SAVI and MSAVI and the GY of soybean cv. AS 3730 IPRO (Agroceres), possibly due to the use of soil effect correction to estimate these VIs (Hatfield & Prueger, 2010). SAVI, MSAVI, and MTVI are directly related to soil reflectance, crop canopy sensitivity, vegetation cover, and chlorophyll absorption (Haboudane et al., 2004).

Linear regression performed with the VIs selected as the most significant in the correlation analysis ($r \geq 0.8$) indicated that EVI-2, EVI, RDVI, and SAVI were promising for estimating GY (Figure 3). EVI-2 was more efficient in estimating the GY of the cv. BRS-8980 ($R^2 = 0.715$; $SEE = 324.85 \text{ kg ha}^{-1}$). The worst fit for the regression models was the SAVI vegetation index ($R^2 = 0.70$; $SEE = 332.83 \text{ kg ha}^{-1}$) (Figure 3). It is important to emphasize the ability of the linear regression models to better estimate cv. BRS-8980 GY, demonstrated by the lower SEE values obtained by the regression models.

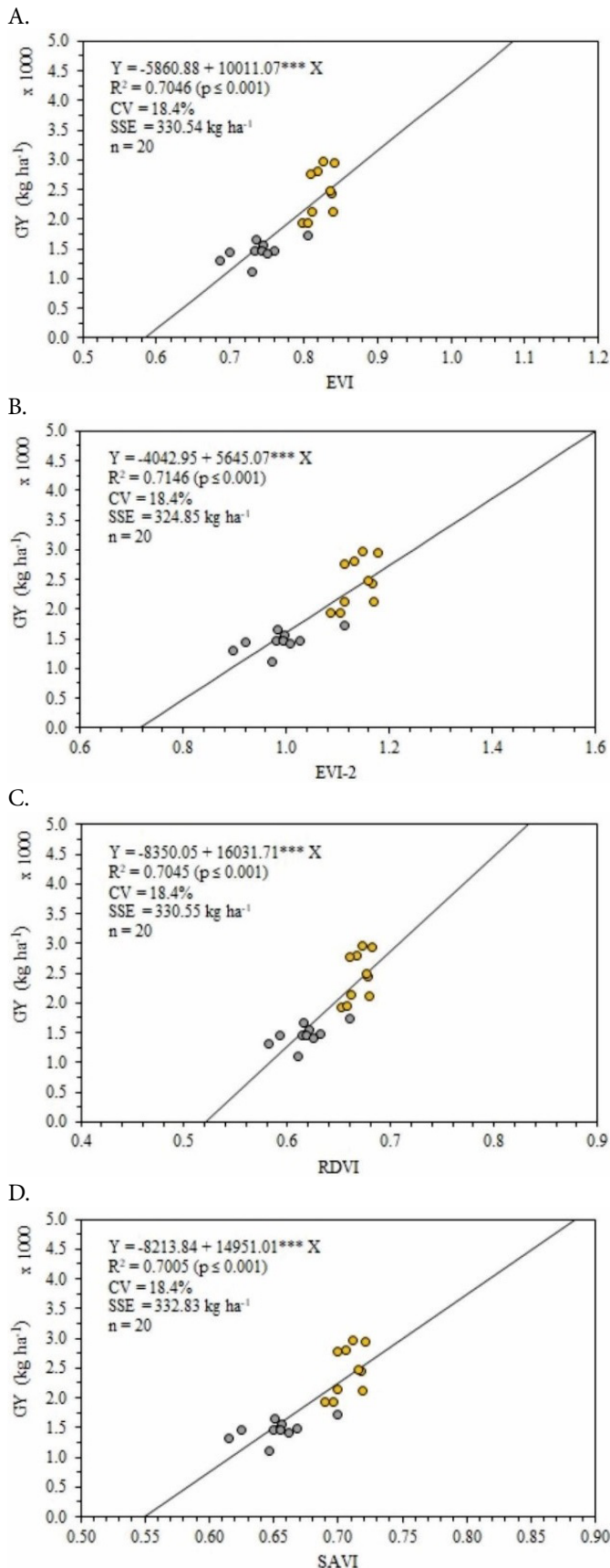
The VIs that best estimated GY were those that used the bands in the NIR, red, and red-edge regions to express the spectral response of soybean to the treatments applied (water regimes and soil N levels). A similar trend was observed by Christenson et al. (2016), who concluded that yield prediction models using VIs that adopt the red, NIR, and red-edge spectral bands better explained grain yield variability among soybean genotypes.

Christenson et al. (2016) generated a GY prediction model using different VIs for soybean cultivars grouped into two maturity groups (G3 and G4). The authors found that the resulting model exhibited $R^2 = 0.58$ and $SEE = 703.0 \text{ kg ha}^{-1}$, performance indices lower than those obtained with the models generated in the present study. The authors attribute this poor performance to the fact that the model was generated for the

Table 4. Pearson's correlation between vegetation indices (VIs) and soybean grain yield (GY, kg ha^{-1}) (n = 20)

VI#	r	VI	r	VI	r	VI	r	VI	r
CI-RED	0.789***	GCI	0.802***	MNGRD	-0.032 ^{ns}	OSAVI	0.828***	RVI	0.789***
CVI	0.709***	GNDVI	0.781***	NDRE	0.803***	PSND	0.707***	SAVI	0.837***
EVI	0.839***	GRVI	0.802***	NDVI	0.757***	RDVI	0.839***	SCCCI	0.793***
EVI-2	0.845***	MEXG	-0.470**	NGRD	-0.074 ^{ns}	RECI	0.816***	TGI	-0.542**

* For description of VIs see Table 3. Significance levels (t-test): ns - Not significant; * - $p \leq 0.05$; ** - $p \leq 0.01$; *** - $p \leq 0.001$



Significance levels according to the t-test: *** - $p \leq 0.001$; ** - $p \leq 0.01$; * - $p \leq 0.05$; ns - Not significant; R² - Coefficient of determination; SEE - Standard error of estimate and n - number of data pairs (50% ETC - gray circles; 100% ETC - orange circles)

Figure 3. Linear regression between promising vegetation indices (VIs) and grain yield (GY) of soybean cv. BRS-8980

clustering of all genotypes from different maturity groups, a strategy that was avoided in the present study.

Validation of the linear regression models showed that among the promising VIs in predicting soybean GY, cv BRS-8980 stood out as the most efficient (higher R² associated with lower RMSE and nRMSE values). The VIs that performed best were EVI-2, RDVI, EVI and SAVI, with RMSE, and nRMSE values ranging from 303.55 kg ha⁻¹ and 15.5% (R² = 0.727), respectively, for the model generated with EVI-2, at 309.25 kg ha⁻¹, and 15.8% (R² = 0.718), for the model generated with SAVI (Figure 4).

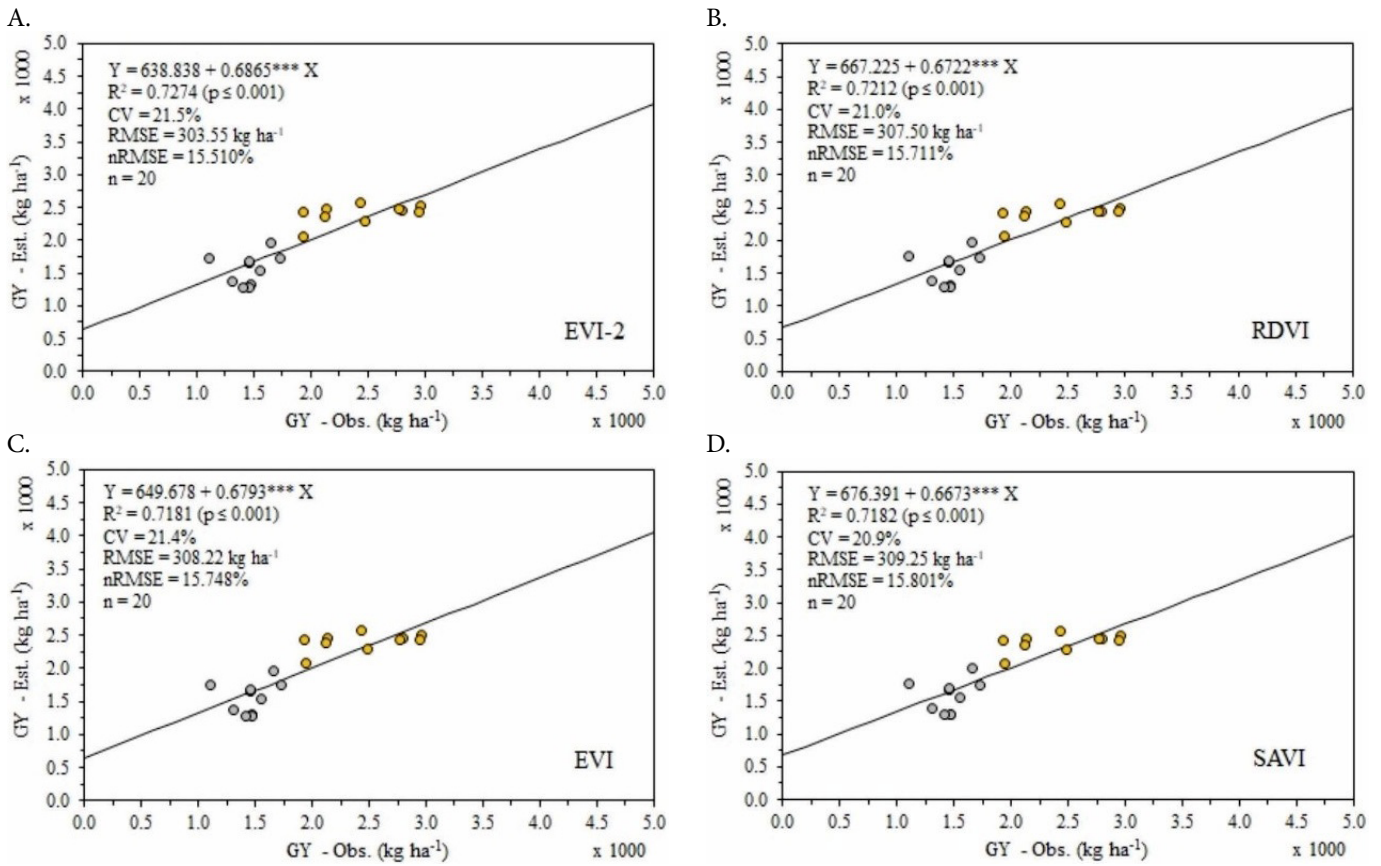
Holzman et al. (2014) conducted a study to estimate soybean grain yield at a regional scale in the Pampas region of Argentina using the temperature vegetation dryness index (TDVI) generated from EVI and surface temperature (Ts). Despite the regional scope of the study, the model proved to be effective in predicting GY. Depending on the agro-climatic zone, the R² values ranged from 0.68 to 0.79, with RMSEs of 366 and 380 kg ha⁻¹ and nRMSEs of 12.0 to 13.0%, respectively, very close to those obtained in the present study. The authors concluded that there is a strong correlation between TDVI and soil moisture measurements, with R² values ranging from 0.61 to 0.83, as well as adequate agreement with the spatial pattern of soil moisture, which explains the good performance of the model.

Maimaitjiang et al. (2020) evaluated the joint use of RGB, multispectral, and thermal sensors embedded in RPAs to estimate soybean grain yield using artificial neural networks. The authors concluded that the most accurate GY estimate (R² = 0.72; RMSE = 478.9 kg ha⁻¹; nRMSE = 15.9%) was obtained with the combined use of all the sensors evaluated. However, it is noteworthy that they also obtained adequate accuracy (R² = 0.52; RMSE = 630.5 kg ha⁻¹; nRMSE = 20.9%) using only multispectral sensors, confirming the results obtained in the present study.

Figure 5 shows the spatial variability of the GY generated with the EVI-2, RDVI, EVI, and SAV VIs, with better performance in estimating GY in response to the water regimes evaluated (WR-50% ETC and WR-100% ETC). The maps show considerable similarity to each other for the same water regime. The maps of GY at WR = 50% ETC show areas with a greater predominance of zones with GY below 1500-2000 kg ha⁻¹, while under WR = 100% ETC, the areas with greater predominance of GY are above 2000-2500 kg ha⁻¹ (Figure 5).

The level of soil water availability for plants directly affects soybean grain yield. Gava et al. (2015) found that imposing a water deficit of 70% ETC throughout the growing season reduced the growth and quality of grains per plant, lowering grain yield. According to Vivan et al. (2013), grain yield increases with the application of the ideal irrigation depth required by the crop. The irrigation depth with full ETC replacement was 511.9 mm (Table 2). Studies indicate that, depending on the soil conditions, climate, sowing date and cultivar, soybean requires an irrigation depth of 450 to 850 mm during the growing season to achieve maximum grain yield (Allen et al., 1998).

Distribution of the prediction errors of the soybean GY estimation models showed spatial clustering patterns at different levels as a function of the water regimes and N levels applied to the soil (Table 5 and Figure 6). Moran's I



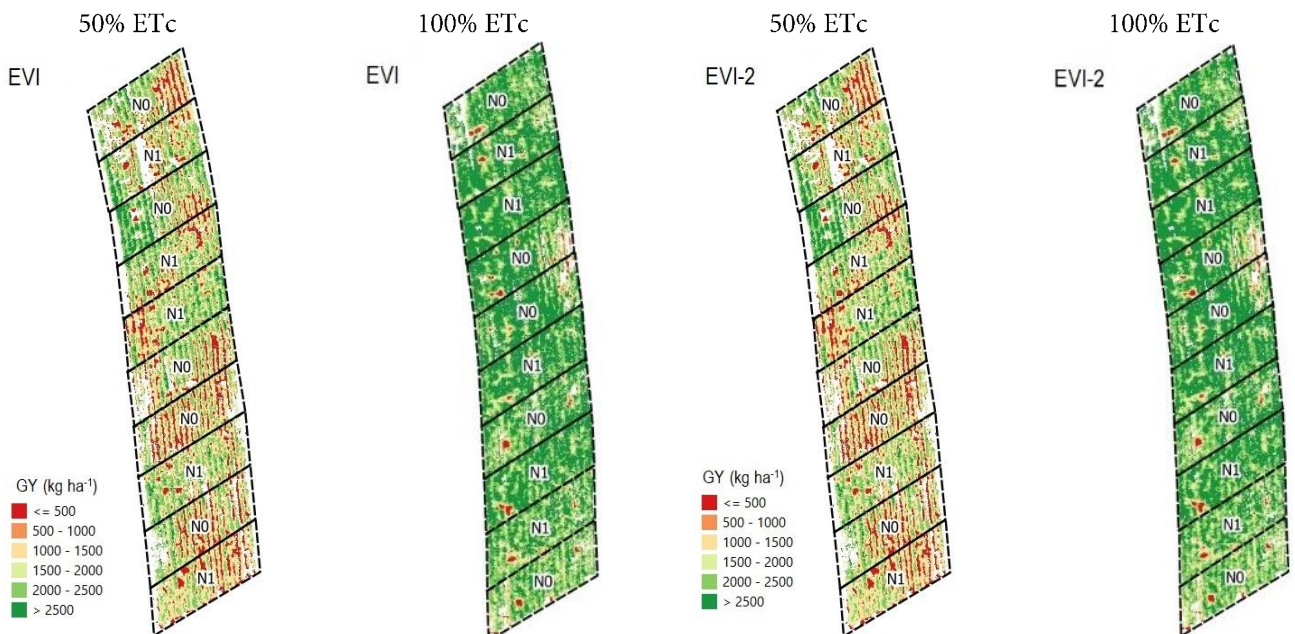
Significance levels according to the t-test: *** - $p \leq 0.001$; ** - $p \leq 0.01$; * - $p \leq 0.05$; ns - Not significant. RMSE - Root mean square error and n - Number of data pairs (50% ETc - gray circles; 100% ETc - orange circles)

Figure 4. Linear regression between cv. BRS-8980 soybean grain yield values measured in the field (GY-Obs.) and estimated by linear regression models (GY-Est.) generated with the vegetation indices (VIs) extracted from the validation dataset

values range from -1 to 1, showing negative to positive spatial autocorrelation, respectively, with values close to zero and significant, indicating spatial randomness, where greater randomness indicates better regression model performance (Maimaitijiang et al., 2020).

The soybean GY prediction models based on EVI-2 provided the smallest average prediction errors (RMSE and

nRMSE), ranging from 149.68 kg ha⁻¹ (nRMSE = 8.31%) (N0) to 173.96 kg ha⁻¹ (nRMSE = 10.24%) (N1) (Table 5). The better performance and spatial randomness of these models in predicting GY (Figure 6) occurs because they use the bands in the NIR, red, and red-edge regions to express the spectral response of soybean to the spatial variability of the water regimes and soil N levels (Christenson et al., 2016).



Continues on the next page

Continuation of Figure 5

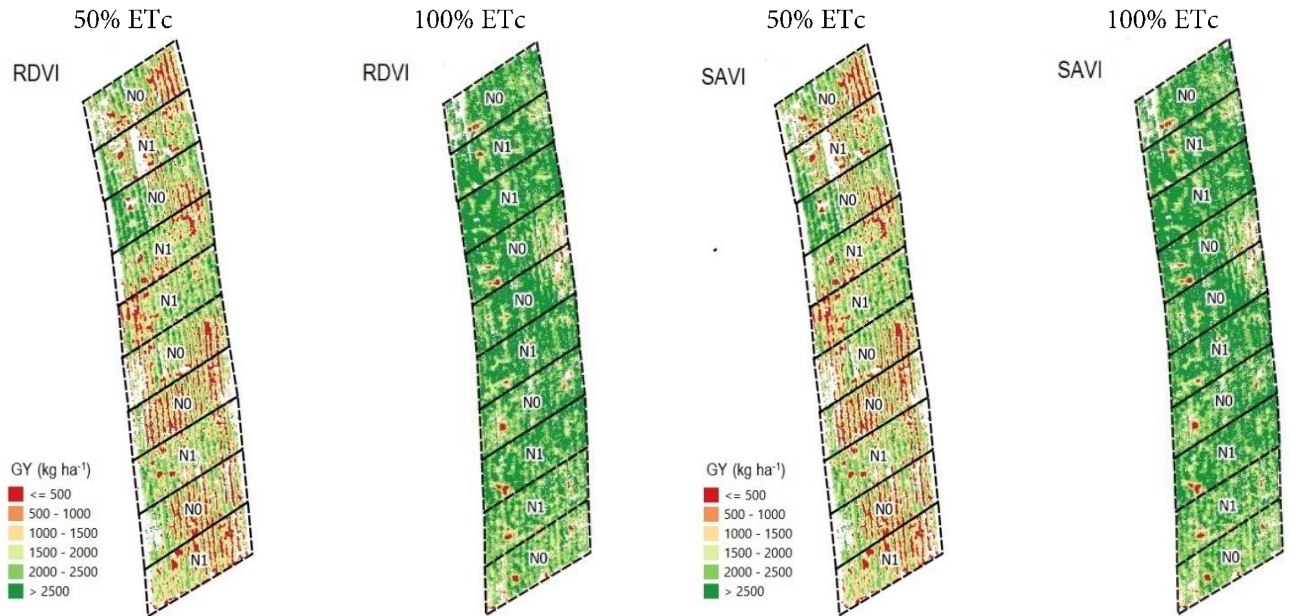


Figure 5. Yield maps of soybean cv. BRS-8980, generated with the promising vegetation indices (VIs), in response to the water regimes evaluated (50 and 100% ETc)

Table 5. Spatial autocorrelation metrics (Global Moran’s I, RMSE and nRMSE) obtained with the regression models for estimating the GY of cv. BRS-8980 with promising vegetation indices (VIs) in response to the N levels evaluated

IV#	Metrics	N0	N1	All	IV#	N0	N1	All	
EVI	Moran’s I	-0.01449 ^{ns}	-0.01449*	-0.00719 ^{ns}	RDVI	-0.01449 ^{ns}	-0.01449 ^{ns}	-0.00719 ^{ns}	
	RMSE	Q1	84.86	79.81		82.34	85.27	69.98	77.62
		Med.	147.46	177.39		162.42	150.65	177.12	163.88
		Q3	188.52	233.13		214.27	191.12	234.47	210.05
	nRMSE	Q1	3.88	4.87		4.27	5.19	5.67	5.40
		Med.	8.19	10.53		9.36	15.17	20.72	17.94
Q3		10.04	12.75	11.91	16.91	30.69	23.84		
EVI-2	Moran’s I	-0.01449***	-0.01449*	-0.00719*	SAVI	-0.01449***	-0.01449 ^{ns}	-0.00719 ^{ns}	
	RMSE	Q1	73.82	71.26		72.81	88.36	77.02	82.69
		Med.	149.68	173.96		161.82	150.87	179.64	165.25
		Q3	186.77	237.07		213.30	192.01	239.00	217.94
	nRMSE	Q1	4.23	4.27		4.25	3.94	5.09	4.43
		Med.	8.31	10.24		9.27	8.39	10.73	9.56
Q3		10.19	13.39	11.81	10.40	13.20	12.46		

* For description of IV see Table 3. Moran’s I: Global Moran’s spatial correlation index (Eq. 5); RMSE - Root mean square error (kg ha⁻¹) (Eq. 3); nRMSE - Normalized root mean square error (kg ha⁻¹) (Eq. 4); Q1 - Lower quartile; Med - Mean; Q3 - Upper quartile; Pseudo p-values: *** - p ≤ 0.001; ** - p ≤ 0.01; * - p ≤ 0.05; ° - p ≤ 0.1; ns - Not significant

The global Moran’s index values obtained for the GY prediction model generated with the EVI-2 VI were low and statistically significant for all N levels, ranging from -0.01449, for N0 (p ≤ 0.001) and N1 (p ≤ 0.05) separately, to -0.00719 (p ≤ 0.05), for all N levels (Table 5 and Figure 6). This indicates that the model generated a low spatial clustering pattern for GY prediction errors, that is, high model randomness (Figure 6).

However, the values of the global Moran’s index obtained for the EVI and SAVI models only indicated high randomness in the prediction of soybean GY with and without N supplementation, respectively, and should not be used, given the limitation of the models for this specific condition. For prediction models based on the RDVI, there was no spatial randomness for any of the conditions evaluated (Table 5). The models should be able to express the GY prediction randomness of different soybean cultivars in any environmental condition (Li et al., 2014).

In a study of soybean grain yield prediction based on the aerial images of RGB, multispectral and thermal sensors associated with different deep learning network methods,

Maimaitijiang et al. (2020) found Moran’s I values in relation to grain yield model prediction errors ranging from 0.028 to 0.144 (p ≤ 0.001) when using the ‘inverse distance’ clustering method, and 0.045 to 0.153 (p ≤ 0.001) with the ‘contiguity edges’ method. They concluded that the fusion of all imaging strategies led to the weakest clustering pattern of prediction errors of all regression models evaluated, indicating that the joint adoption of all multimodal data can improve the adaptability of the model in space by weakening the spatial clustering of prediction errors.

Evaluation of the grain yield prediction model based on EVI-2 indicated that the lowest local Moran’s index values (≤ 0.005), with significant pseudo-p-values (p ≤ 0.05), were observed equally in the subplots with and without N supplementation, with 35 and 33 subplots, respectively. The evaluation of all subplots (N0 and N1) revealed that the lowest local Moran’s I (≤ 0.005) were observed in 78 subplots, 61 of which had pseudo-p-values less than 5% (p ≤ 0.05), indicating high spatial randomness of the soybean grain yield prediction model (Figure 6).

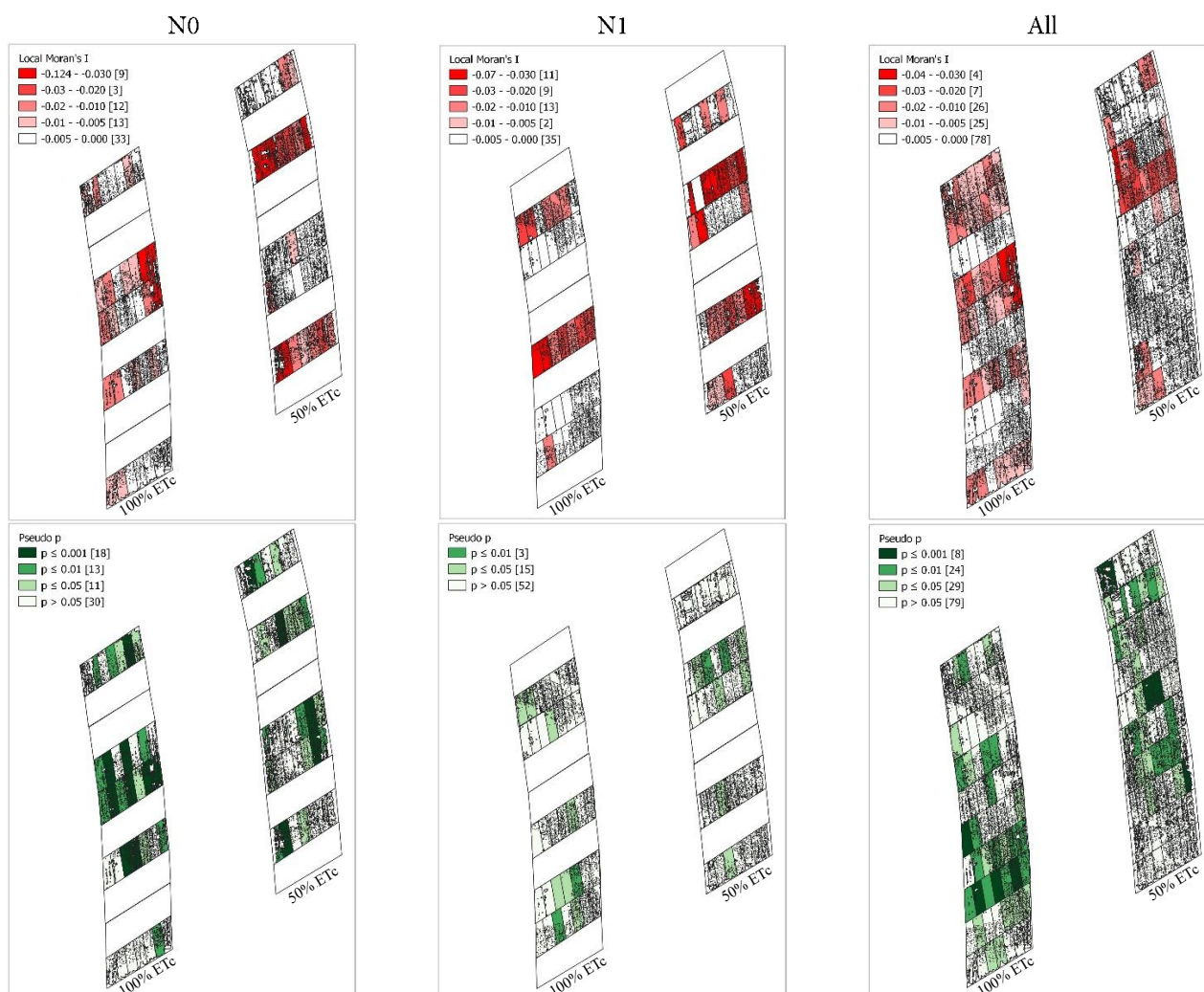


Figure 6. Local Moran's spatial autocorrelation index (I) and pseudo-p-values for the grain yield of soybean cv. BRS-8980, generated with the promising vegetation index - (EVI-2), in response to the N levels evaluated (with - N1 and without - N0 supplementation)

Maimaitijiang et al. (2020) found a better spatial distribution pattern of the residuals of the soybean grain yield prediction models, with values ranging from 50 to 400 kg ha⁻¹, with the joint use of RGB, multispectral, and thermal sensors embedded in the UAV under study to estimate grain yield using artificial neural networks. The authors attributed this superior performance to better efficacy and high randomness in spatial correlation, represented by the low Moran's I values of these prediction models.

The spatial pattern of grain yield variability is conditioned by spatial factors (soil properties, irrigation management, and crop practices), temporal factors (soil pathogens, diseases, and crop production problems) (Peralta et al., 2016), and the cultivars studies (Haghighattalab et al., 2017). Thus, the importance of evaluating spatial autocorrelation in studies proposing prediction models for soybean GY is due to the risk of inaccurate estimates, distorted variance or, more importantly, erroneous conclusions (Peralta et al., 2016).

The superior performance of the soybean GY prediction models may also be related to the development stage of the cultivar used to generate the GY prediction models. In this study, aerial images obtained at the R5 stage were used to create the GY prediction models. Several studies have shown that the ideal stage of soybean development for predicting grain

yield is between flowering and initial grain filling (stages R2 to R5) (Gao et al., 2018). In particular, the initial stage of grain filling (R5) was considered the best for predicting grain yield (Zhang et al., 2019).

CONCLUSION

The soybean grain yield prediction model based on EVI-2 exhibits high spatial randomness, for all evaluated treatments, and smaller prediction errors of 149.68 kg ha⁻¹ (without N supplementation) and 173.96 kg ha⁻¹ (with N supplementation).

LITERATURE CITED

- Allen, R. G.; Pereira, L. S.; Raes, D.; Smith, M. Crop evapotranspiration: Guidelines for computing crop water requirements. Rome: FAO, 300p. 1998. Drainage and Irrigation Paper, 56
- Anselin, L. Local indicators of spatial association - LISA. *Geographical Analysis*, v.27, p.93-115, 1995. <https://doi.org/10.1111/j.1538-4632.1995.tb00338.x>
- Anselin, L.; Syabri, I.; Kho, Y. GeoDA: An introduction to spatial data analysis. *Geographical Analysis*, v.38, p.5-22, 2006. <https://doi.org/10.1111/j.0016-7363.2005.00671.x>

- Baio, F. H. R.; Neves, D. C.; Campos, C. N. da S.; Teodoro, P. E. Relationship between cotton productivity and variability of NDVI obtained by Landsat images. *Bioscience Journal*, v.34 (suplemento 1), p.197-205, 2018. <https://doi.org/10.14393/BJ-v34n6a2018-39583>
- Barbedo, J. G. A. A Review on the use of unmanned aerial vehicles and imaging sensors for monitoring and assessing plant stresses. *Drones*, v.3, p.1-27, 2019. <https://doi.org/10.3390/drones3020040>
- Bendig, J.; Yu, K.; Aasen, H.; Bolten, A.; Bennertz, S.; Broscheit, J.; Gnyp, M.L.; Bareth, G. Combining UAV-based plant height from crop surface models, visible, and near infrared vegetation indices for biomass monitoring in barley. *International Journal of Applied Earth Observation and Geoinformation*, v.39, p.79-87, 2015. <https://doi.org/10.1016/j.jag.2015.02.012>
- Blackburn, G. A. Quantifying chlorophylls and carotenoids at leaf and canopy scales: An evaluation of some hyperspectral approaches. *Remote Sensing of Environment*, v.66, p.273-285, 1998. [https://doi.org/10.1016/S0034-4257\(98\)00059-5](https://doi.org/10.1016/S0034-4257(98)00059-5)
- Burgos-Artizzu, X. P.; Ribeiro, A.; Guijarro, M.; Pajares, G. Real-time image processing for crop/weed discrimination in maize fields. *Computers and Electronics in Agriculture*, v.75, p.337-346, 2011. <https://doi.org/10.1016/j.compag.2010.12.011>
- Christenson, B. S.; Schapaugh Jr., W. T.; An, N.; Price, K. P.; Prasad, V.; Fritz, A. K. Predicting soybean relative maturity and seed yield using canopy reflectance. *Crop Science*, v.56, p.625-643, 2016. <https://doi.org/10.2135/cropsci2015.04.0237>
- Dalposso, G. H.; Uribe-Opazo, M. A.; Mercante, E.; Lamparelli, R. A. C. Spatial autocorrelation of NDVI and GVI indices derived from LANDSAT/TM images for soybean crops in the western of the State of Paraná in 2004/2005 crop season. *Engenharia Agrícola*, v.33, p.525-537, 2013. <https://doi.org/10.1590/S0100-69162013000300009>
- Dong, J.; Xiao, X.; Wagle, P.; Zang, G.; Zhou, Y.; Jin, C.; Torn, M. S.; Meyers, T. P.; Suyker, A. E.; Wang, J.; Yan, H.; Biradar, C.; Moore, B. Comparison of four EVI-based models for estimating gross primary production of maize and soybean croplands and tallgrass prairie under severe drought. *Remote Sensing of Environment*, v.162, p.154-168, 2015. <https://doi.org/10.1016/j.rse.2015.02.022>
- Gao, F.; Anderson, M. C.; Daughtry, C.; Johnson, D. M. Assessing the variability of corn and soybean yields in central Iowa using high spatiotemporal resolution multi-satellite imagery. *Remote Sensing*, v.10, p.1489, 2018. <https://doi.org/10.3390/rs10091489>
- Gava, R.; Frizzzone, J. A.; Snyder, R. L.; José, J. V.; Fraga Junior, E. F.; Perboni, A. Estresse hídrico em diferentes fases da cultura da soja. *Revista Brasileira de Agricultura Irrigada*, v.9, p.349-359, 2015. <https://doi.org/10.7127/rbai.v9n600368>
- Ghulam, A.; Ghulam, O.; Maimaitijiang, M.; Freeman, K.; Porton, I.; Maimaitiyiming, M. Remote sensing based spatial statistics to document tropical rainforest transition pathways. *Remote Sensing*, v.7, p.6257-6279, 2015. <https://doi.org/10.3390/rs70506257>
- Gitelson, A. A.; Viña, A.; Ciganda, V.; Rundquist, D. C.; Arkebauer, T. J. Remote estimation of canopy chlorophyll content in crops. *Geophysical Research Letters*, v.32, p.1-4, 2005. <https://doi.org/10.1029/2005GL022688>
- Haboudane, D.; Miller, J. R.; Pattey, E.; Zarco-Tejada, P. J.; Strachan, I. B. Hyperspectral vegetation indices and novel algorithms for predicting green LAI of crop canopies: modeling and validation in the context of precision agriculture. *Remote Sensing of Environment*, v.90, p.337-352, 2004. <https://doi.org/10.1016/j.rse.2003.12.013>
- Haghighattalab, A.; Crain, J.; Mondal, S.; Rutkoski, J.; Singh, R. P.; Poland, J. Application of geographically weighted regression to improve grain yield prediction from unmanned aerial system imagery. *Crop Science*, v.57, p.2478-2489, 2017. <https://doi.org/10.2135/cropsci2016.12.1016>
- Hamuda, E.; Glavin, M.; Jones, E. A survey of image processing techniques for plant extraction and segmentation in the field. *Computers and Electronics in Agriculture*, v.125, p.184-199, 2016. <https://doi.org/10.1016/j.compag.2016.04.024>
- Hassan, M. A.; Yang, M.; Rasheed, A.; Yang, G.; Reynolds, M.; Xia, X.; Xiao, Y.; He, Z. A rapid monitoring of NDVI across the wheat growth cycle for grain yield prediction using a multi-spectral UAV platform. *Plant Science*, v.282, p.95-103, 2019. <https://doi.org/10.1016/j.plantsci.2018.10.022>
- Hatfield, J. L.; Prueger, J. H. Value of using different vegetative indices to quantify agricultural crop characteristics at different growth stages under varying management practices. *Remote Sensing*, v.2, p.562-578, 2010. <https://doi.org/10.3390/rs2020562>
- Holzman, M. E.; Rivas, R.; Piccolo, M. C. Estimating soil moisture and the relationship with crop yield using surface temperature and vegetation index. *International Journal of Applied Earth Observations and Geoinformation*, v.28, p.181-192, 2014. <https://doi.org/10.1016/j.jag.2013.12.006>
- Hungria, M.; Campo, R. J.; Mendes, I. C. Fixação biológica do nitrogênio na soja. *Circular Técnica*, 35. Londrina: Embrapa Soja, 2001. 48p.
- Hunt, E. R.; Daughtry, C. S. T. What good are unmanned aircraft systems for agricultural remote sensing and precision agriculture? *International Journal of Remote Sensing*, v.39, p.5345-5376, 2018. <https://doi.org/10.1080/01431161.2017.1410300>
- Hunt, E. R.; Daughtry, C. S. T.; Eitel, J. U. H.; Long, D. S. Remote sensing leaf chlorophyll content using a visible band index. *Agronomy Journal*, v.103, p.1090-1099, 2011. <https://doi.org/10.2134/AGRONJ2010.0395>
- INMET - Instituto Nacional de Meteorologia. Dados históricos: 2019. Available on: <<https://portal.inmet.gov.br/dadoshistoricos>>. Accessed on: Apr. 2020.
- Jiang, Z.; Huete, A.; Miura, T.; Didan, K. Development of a two-band enhanced vegetation index without a blue band. *Remote Sensing of Environment*, v.112, p.3833-3845, 2008. <https://doi.org/10.1016/j.rse.2008.06.006>
- Li, L.; Zang, Q.; Huang, D. A review of imaging techniques for plant phenotyping. *Sensors*, v.14, p.20078-20111, 2014. <https://doi.org/10.3390/s141120078>
- Maimaitijiang, M.; Sagan, V.; Sidike, P.; Hartling, S.; Esposito, F.; Fritschi, F. B. Soybean yield prediction from UAV using multimodal data fusion and deep learning. *Remote Sensing of Environment*, v.237, p.111599, 2020. <https://doi.org/10.1016/j.rse.2019.111599>
- Medeiros, M. R. de; Cavalcanti, E. P.; Duarte, J. F. de M. Classificação climática de Köppen para o Estado do Piauí- Brasil. *Revista Equador*, v.9, p.82-99, 2020.
- Melo, F. de B.; Andrade Junior, A. S. de; Pessoa, B. L. de O. Levantamento, zoneamento e mapeamento pedológico detalhado da área experimental da Embrapa Meio-Norte em Teresina, PI. Teresina: Embrapa Meio-Norte, 34p. 2014.

- Nguy-Robertson, A.; Gitelson, A.; Peng, Y.; Viña, A.; Arkebauer, T.; Rundquist, D. Green leaf area index estimation in maize and soybean: combining vegetation indices to achieve maximal sensitivity. *Agronomy Journal*, v.104, p.1336-1347, 2012. <https://doi.org/10.2134/AGRONJ2012.0065>
- Peralta, N. R.; Assefa, Y.; Du, J.; Barden, C. J.; Ciampitti, I. A. Mid-season high-resolution satellite imagery for forecasting site-specific corn yield. *Remote Sensing*, v.8, p.848, 2016. <https://doi.org/10.3390/rs8100848>
- QGIS Development Team. 2021. QGIS User Guide, Release 3.16. Available on: <<https://docs.qgis.org/3.16/en/docs/index.html>>. Accessed on: Mar. 2021.
- Raper, T. B.; Varco, J. J. Canopy-scale wavelength and vegetative index sensitivities to cotton growth parameters and nitrogen status. *Precision Agriculture*, v.16, p.62-76, 2015. <https://doi.org/10.1007/s11119-014-9383-4>
- Rondeaux, G.; Steven, M.; Baret, F. Optimization of soil-adjusted vegetation indices. *Remote Sensing of Environment*, v.55, p.95-107, 1996. [https://doi.org/10.1016/0034-4257\(95\)00186-7](https://doi.org/10.1016/0034-4257(95)00186-7)
- Roujean, J. L.; Breon, F. M. Estimating PAR absorbed by vegetation from bidirectional reflectance measurements. *Remote Sensing of Environment*, v.51, p.375-384, 1995. [https://doi.org/10.1016/0034-4257\(94\)00114-3](https://doi.org/10.1016/0034-4257(94)00114-3)
- Silva, S. P. Crescimento e produtividade da soja em resposta a adubação nitrogenada com e sem deficiência hídrica. Teresina: UFPI, 2021. 80p. Dissertação Mestrado
- Silva Junior, C. A. da; Nanni, M. R.; Shakir, M.; Teodoro, P. E.; Oliveira-Junior, J. F. de; Cezar, E.; Gois, G. de; Lima, M.; Wojciechowski, J. C.; Shiratsuchig, L. S. Soybean varieties discrimination using non-imaging hyperspectral sensor. *Infrared Physics and Technology*, v.89, p.338-350. 2018. <https://doi.org/10.1016/j.infrared.2018.01.027>
- Sripada, R. P.; Heiniger, R. W.; White, J. G.; Meijer, A. D. Aerial color infrared photography for determining early in-season nitrogen requirements in corn. *Agronomy Journal*, v.98, p.968-977, 2006. <https://doi.org/10.2134/agronj2005.0200>
- Schwalbert, R. A.; Amado, T.; Corassa, G.; Pott, L. P.; Prasad, P. V. V.; Ciampitti, I. A. Satellite-based soybean yield forecast: integrating machine learning and weather data for improving crop yield prediction in southern Brazil. *Agricultural Forest and Meteorology*, v.284, 107886, 2020. <https://doi.org/10.1016/j.agrformet.2019.107886>
- Vincini, M.; Frazzi, F.; D'Alessio, P. A broad-band leaf chlorophyll vegetation index at the canopy scale. *Precision Agriculture*, v.9, p.303-319, 2008. <https://doi.org/10.1007/s11119-008-9075-z>
- Vivan, G. A.; Peiter, M. X.; Robaina, A. D.; Barboza, F. da S.; Buske, T. Rendimento relativo da cultura da soja em função da lâmina de irrigação. *Irriga*, v.18, p.282-292, 2013. <https://doi.org/10.15809/irriga.2013v18n2p282>
- Wang, L.; Tian, Y.; Yao, X.; Zhu, Y.; Cao, W. Predicting grain yield and protein content in wheat by fusing multi-sensor and multi-temporal remote-sensing images. *Field Crops Research*, v.164, p.178-188, 2014. <https://doi.org/10.1016/j.fcr.2014.05.001>
- Xue, J.; Su, B. Significant remote sensing vegetation indices: a review of developments and applications. *Journal Sensors*, v.2017, p.1-17, 2017. <https://doi.org/10.1155/2017/1353691>
- Zaiontz, C. Real statistics using Excel. Available on: <<http://www.real-statistics.com>>. Accessed on: Mar. 2020.
- Zhang, X.; Zhao, J.; Yang, G.; Liu, J.; Cao, J.; Li, C.; Zhao, X.; Gai, J. Establishment of plot-yield prediction models in soybean breeding programs using UAV-based hyperspectral remote sensing. *Remote Sensing*, v.11, p.2752, 2019. <https://doi.org/10.3390/rs11232752>
- Zhao, Y.; Potgieter, A. B.; Zhang, M.; Wu, B.; Hammer, G. L. Predicting wheat yield at the field scale by combining high-resolution Sentinel-2 satellite imagery and crop modelling. *Remote Sensing*, v.12, p.1-20, 2020. <https://doi.org/10.3390/rs12061024>
- Zhong, L.; Hu, L.; Zhou, H. Deep learning based multi-temporal crop classification. *Remote Sensing of Environment*, v.221, p.430-443, 2019. <https://doi.org/10.1016/j.rse.2018.11.032>